RSC Advances

PAPER

View Article Online
View Journal | View Issue

Cite this: *RSC Adv.*, 2022, **12**, 5522

Characteristic analysis of three-ecofriendly reduced graphene oxides (rGOs) and their application in water–ethanol-based fluids with different volume ratios

Jun Xu,[a] Lingchao Lu,[a] Guangbin Duan[b] and Weilin Zhao*[b]

In this paper, three-ecofriendly reduced graphene oxides (rGOs) were obtained by using three green reducing agents (beer, wine and cocoa) to reduce the graphene oxide (GO), and were labeled as B-rGO, W-rGO and C-rGO. Meanwhile, rGO nanofluids with different water–ethanol volume ratios (25 : 75, 50 : 50, 75 : 25) were prepared based on three-ecofriendly rGOs. The structure properties of the three-ecofriendly rGOs were investigated by XRD, FR-IT, Raman spectroscopy and XPS analysis. Meanwhile, the thermophysical properties of rGO nanofluids were analyzed. Experimental results indicated that the stability and thermophysical properties of rGO nanofluids were slightly different, indicating that the properties of the nanofluids are dependent on the type of base fluids and nanoparticles. When the water–ethanol volume ratio was maintained at 25 : 75, the stability experiment results showed that W-rGO nanofluids presented excellent stability, which indirectly confirmed their excellent thermal conductivity. Furthermore, the contact angle experiment indicated that the contact angles of rGO nanofluids decreased with the increase of temperature. In a word, these three rGOs and their nanofluids exhibited preferable properties that make them promising in the field of heat transfer.

Received 1st January 2022
Accepted 9th February 2022

DOI: 10.1039/d2ra00007e

rsc.li/rsc-advances

1. Introduction

The appearance of graphene in 2004 caused a sensation in the world, triggering a research boom in various fields.[1] Graphene is a novel carbon-based nanomaterial with excellent optical, electrical and mechanical properties, which is composed of a hexagonal lattice of carbon atoms and sp^2 hybrid orbitals. In view of the above properties, it shows considerable potential for applications in the field of materials science, biomedicine and drug delivery,[2–4] and is regarded as an ideal material for the future.

Graphene has been prepared in a variety of ways, with the earliest development of mechanical stripping and subsequent development of various preparation methods, such as electrochemical exfoliation,[5,6] chemical vapor deposition,[7,8] plasma-assisted ball milling[9] and oxidation–reduction method.[10–12] Among these methods, the REDOX method has the advantage of low cost, high yield, and mass production, which has become one of the effective ways to achieve large-amount preparation of graphene. The main raw materials of REDOX method are GO synthesized by the traditional modified Hummers method[13] and reductants (such as hydrazine hydrate ($N_2H_4 \cdot H_2O$)[14] and sodium borohydride ($NaBH_4$)[15]). However, these reducing agents have different degrees of toxicity and corrosiveness, and the preparation process is easy to cause environmental pollution. Therefore, researchers are working to develop efficient, controllable, friendly and inexpensive reductants. In recent years, various research teams have proposed different types of green reducing agents to replace traditional toxic reducing agents.[16–20] Fan *et al.*[21] used metallic iron as a reducing agent for the large-amount preparation of graphene nanosheets. The experimental results show that after mixing the iron powder and the GO solution evenly, the graphene can be prepared after 6 h reaction at room temperature. Jin *et al.*[16] proposed a method to prepare graphene from sodium carbonate (Na_2CO_3). By X-photoelectron spectroscopy, the carbon–oxygen atom ratio of the graphene prepared after reduction increased from 2.48 to 8.15. Bo *et al.*[22] treated GO with caffeic acid to obtain graphene products. Experimental studies have found that when the ratio of caffeic acid powder to GO powder is 50 : 1 and the reaction time is 24 h, the C/O ratio in the graphene product can reach 7.15, and the contact angle increased from 36° to 92°. Cheng *et al.*[23] used urushiol (an extract of natural sumac) to study the reduction of GO. TGA test results found that the reduced graphene sample has only 8% mass loss at 300 °C. Liu's research group[24] adopted bovine serum albumin as raw material, and GO can be successfully reduced by adjusting the pH of the reaction.

[a]*Key Laboratory of Building Materials Preparation and Testing Technology, University of Jinan, 250022 Jinan, People's Republic of China*
[b]*School of Material Science and Engineering, University of Jinan, 250022 Jinan, People's Republic of China. E-mail: zhaowl_ujn@126.com*

Experimental exploration had further confirmed that graphene nanosheets can be modified with bovine serum albumin, which was embodied as the extracellular matrix embedded on the surface of the graphene sheet. Yari *et al.*[25] proposed using nettle extract synthesize graphene. The experimental results confirmed that the reducibility of nettle is close to hydrazine hydrate, but the graphene product after reduction of nettle has better dispersibility in the polyurethane matrix than hydrazine hydrate.

Graphene has excellent thermal conductivity and is an excellent choice for preparing nanofluids as nano-additives. Experimental studies have shown that the heat conduction efficiency of monolayer graphene is 3000–5000 W (m^{-1} K^{-1}). Li *et al.*[26] researched the supercooling degree of graphene/water nanofluids, and the experimental results indicated that the condensation time of graphene nanofluids with a surface mass fraction of 0.1% was 38% lower than that of the base liquid. Sadri *et al.*[27] prepared GO nanofluids using a two-step method. Their experiments resealed the enhancement of thermal conductivity was 24.18% at 45 °C and viscosity was closer to the distilled water viscosity at low concentrations. Mehrali *et al.*[28] adopted Hummer's method to prepare NDGs, and the influence of NDGs particle concentration on thermal conductivity of NDGs nanofluids was investigated. The results found that the electrical conductivity increased with the increase of NDG nanoparticles concentration, reaching 1814.96%. In general, the common base solutions for nanofluids include water, glycol, and methanol.[29–33] However, the comparative analysis of the properties of graphene prepared with different reducing agents and its water–alcohol mixed-based nanofluid is still relatively rare.

In this paper, the comparative analysis of the properties of graphene prepared with natural reductant (beer, wine, cocoa) and its water–alcohol mixed-based fluids were conducted. The structural differences of the main components of the three natural reducing agents were analyzed, and the microscopic morphology, stability, particle size and thermal conductivity and wettability of the water/ethanol mixed-based fluids of the three prepared reduced graphene oxides were compared. It expected that reduced graphene oxide (rGO) would have a broader application prospect in the field of heat transfer.

2. Experimental section

2.1 Reagents and chemicals

Flake graphite, sodium nitrate ($NaNO_3$), hydrochloric acid (HCl, 37%), sulfuric acid (H_2SO_4, 98%), potassium permanganate ($KMnO_4$, 99.9%), hydrogen peroxide (H_2O_2, 30%), sodium carbonate ($NaCO_3$) and ammonia were procured from Alfa Aesar. All drugs are analytically pure. Beer (Budweiser Beer Co. Ltd, China), wine (Yantai Changyu Grape Brewing Co. Ltd, China) and cocoa (No Sikkim Cocoa Food Co. Ltd, China) are bought from a nearby supermarket and simply purified before be used. The content of tannic acid was determined by tannic acid analysis test method based on Chinese forestry standard LY/T 1642-2005. The content of tannic acid in beer, wine and cocoa was 13.35%, 19.92% and 8.75%, respectively. The water used throughout the experiments was DI-water.

2.2 Preparation of GO

In brief, the steps for the preparation of GO are shown as follows: firstly, flake graphite and $NaNO_3$ were slowly added to H_2SO_4 treated by ice water bath under the action of magnetic stirrer for 5 min. Then after slowly adding $KMnO_4$, the solution turned dark green. The temperature of the whole reaction process should keep under 5 °C. Secondly, the dark green solution was stirred for 2 h at 35 °C, and then added DI-water drop by drop. After that, the water bath temperature rose to 85 °C, the solution color gradually became brown. Thirdly, the brown solution was stirred in 85 °C water bath for 15 min. After added DI-water and H_2O_2, the solution turned into bright yellow. Finally, the bright yellow solution was washed, centrifuged, and dried into GO powder. The flowchart of preparation of GO powder is shown in Fig. 1.

2.3 Preparation of three-ecofriendly rGO

The preparation method of rGO from beer was similar to wine. Firstly, 50 mg GO was dispersed in 50 ml deionized water, and then dispersed evenly by ultrasound and mixed with 200 ml beer or wine the mixed solutions were kept continuously stirring in the oil bath at 90 °C for 10 h. This process requires condensation reflux to allow the reactants to react adequately and avoid loss. In all the synthesis, the final product was washed thoroughly with distilled water and anhydrous ethanol three times, respectively, centrifuged at 10 000 rpm for 5 min, filtered to collect the precipitate, dried in a freeze dryer for 72 h, and grinded into three rGO powders, which were marked as B-rGO and W-rGO.

When cocoa was used as reducing agent, it was necessary to adjust the pH of GO solution to 8 with 3 ml of 25% ammonia solution in advance, and the dosage of cocoa was 2.5 g. Other operation steps were the same as beer and wine. The flowchart of preparation is displayed in Fig. 2.

2.4 Characterization

In this paper, a series of characterization methods were adopted to analyze the morphology and structure of GO and rGO. The morphology and element analysis of the GO and rGO was characterized by field-emission scanning electron microscope (FE-SEM) (Zeiss Sigma 300) and energy spectrum (Smart EDX). The structural properties of GO and rGO was represented by Fourier transform infrared (FT-IR) spectra (Nicolet 380, Thermo, American), Raman analysis (HORIBA Scientific Lab-RAM HR Evolution) and X-ray diffraction (XRD) (D8-ADVANCE, BRUKER, Germany). UV-visible spectrophotometer (UV-3600, Shimadzu, Japan), thermal conductivity meter (KD2-Pro, CEM, American), particle size analyzer (LS-13-320, Beckman Kurt, American) and contact angle meter (JC2000D1, Shanghai, China) were used to analyze the suspension stability, thermal conductivity, particle size and contact angle of rGO nanofluids. Furthermore, the measurement uncertainty of thermal conductivity meter is ±5%, and the measurement accuracy of

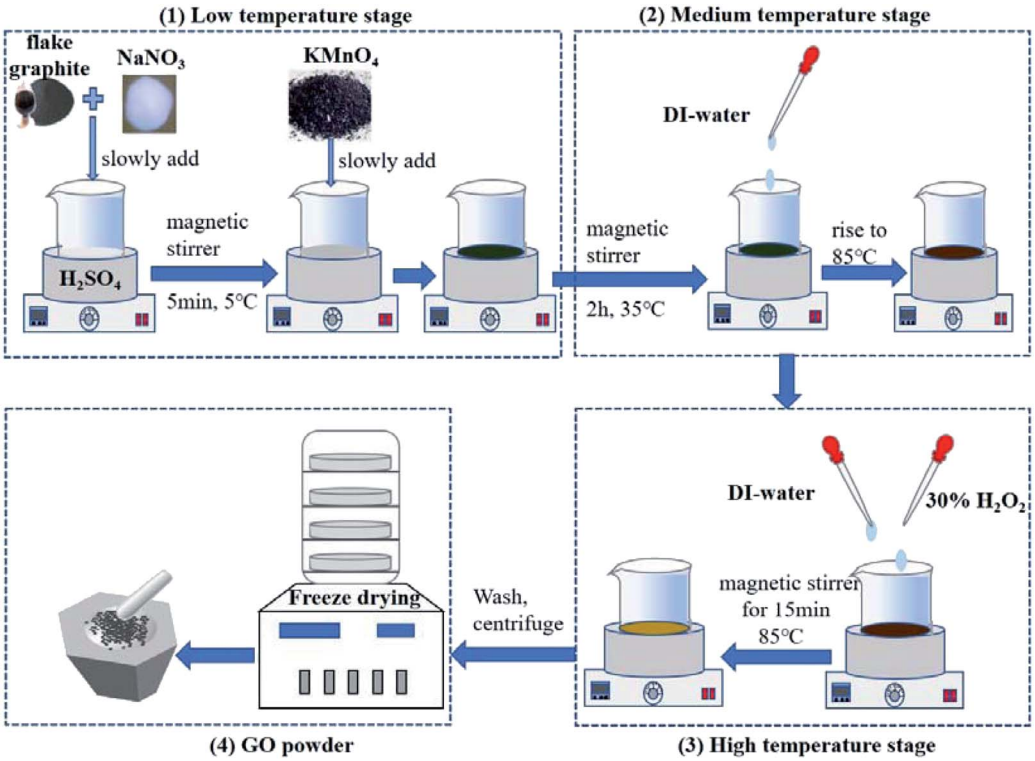

Fig. 1 Flowchart of preparation of GO powder.

contact angle is 0.1°. For accuracy, all data was measured twice to take the average value.

3. Results and discussion

3.1 Characterization analysis of three-ecofriendly rGO

3.1.1 Microstructure analysis of three-ecofriendly rGO. Fig. 3 illustrates SEM images of GO and three-ecofriendly rGO (the inline diagram is mapping analysis). The prepared GO is lamellar and has folds on the surface (Fig. 3(a)). By comparing Fig. 3(b)–(d), it is clear that the microscopic morphology of rGO prepared by three different reducing agents has no obvious difference and retains the folds, which was similar to GO. Moreover, Table 1 displays the weight% and atomic% of element C and O in the mapping analysis, it's clear that GO and rGO mainly contain C and O elements, and after reduction with three reductants, O content is reduced to a certain extent. For example, the weight% of C in GO is 53.72%, the weight% of O is 46.28%, while in W-rGO is 80.57% and 19.43%, which due to the reducing agent makes the hydroxyl group, epoxy group and other groups absorb the electrons of the environment and dehydration.

3.1.2 FT-IR, Raman and XRD analysis of GO and rGO. To investigate the chemical structure of the three rGO, the three kinds of rGO were analyzed by FT-IR spectra. As shown in Fig. 4(a), the absorption peak of GO at wave number 1734, 1452

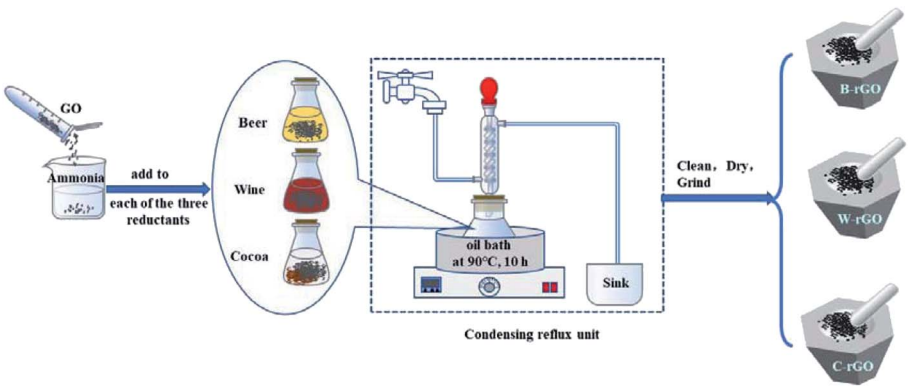

Fig. 2 Flowchart of preparation of three-ecofriendly rGO.

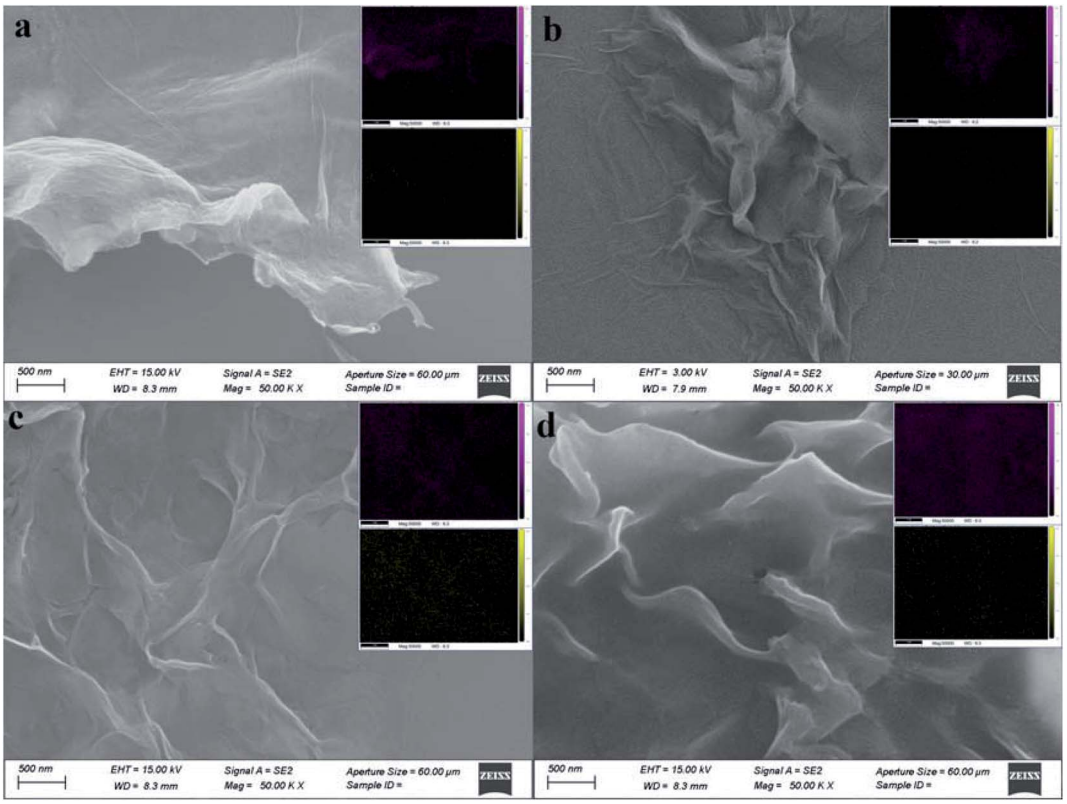

Fig. 3 SEM images: (a) GO, (b) B-rGO, (c) W-rGO, (d) C-rGO.

and 1633 cm^{-1} respectively represent the vibration absorption peak of C=O (carboxyl, epoxy), the stretching vibration peak of C=C and the bending vibration peak of OH. While the band at 1004 cm^{-1} can be assigned to (C–O–C) group.[34] The oxygen-containing bands of C=O, C–O–C and C=C stretching are gradually eliminated with the presence of reducing agents, it can be seen that the peak of oxygen-containing functional groups in the three kinds of rGO is significantly weakened, while the intensity of the hydroxyl band at 3450 cm^{-1} was clearly decremental.[35] Raman test analysis was conducted to further characterize GO and three-ecofriendly rGO. As shown in Fig. 4(b), Raman spectra indicated that there were three main characteristic peaks: the G peak is the main characteristic peak of rGO located near 1592 cm^{-1}, which arise from the in-plane vibration of sp^2 carbon atoms. While the D peak generally regards as the disordered vibration peak of rGO and used to characterize structural defects or edges in rGO samples, which appear at 1353 cm^{-1}. The more defects there are in the preparation and composite process, the stronger the strength of D peak is. The strength ratio of I_D/I_G serves as a measure of the disorder degree of rGO carbon nanomaterials. Meanwhile, the intensity ratio (I_D/I_G) of GO was 0.89, the I_D/I_G of B-rGO, W-rGO and C-rGO was 0.93, 1.08 and 0.95, respectively. The variational strength ratio may be mainly due to the reduction of rGO with the introduction of reducing agent, which increases the order degree of graphene.[36] In addition, the XRD patterns of graphite, GO and rGO were shown in Fig. 4(c) and (d). It can be seen from Fig. 6 that the natural graphite powder has a sharp and strong diffraction peak at $2\theta = 26°$, corresponding to the characteristic diffraction peak of graphite. In contrast, the diffraction peak at $2\theta = 10.2°$ is a characteristic peak of GO and corresponds to the (002) crystal plane. Furthermore, when GO was reduced to rGO, the diffraction peak of the crystal plane (002) of GO disappears, and a new diffraction peak appears at around $2\theta = 23°$ and shows the initial amorphous structure, indicating that the functional groups of GO have been efficiently eliminated.[35] The XRD characterization results of the reported graphene are consistent, further illustrating the formation of rGO.[37,38] At the

Table 1 The weight% and atomic% of element C and O in the mapping analysis

	C (weight%)	C (atomic%)	Error%	O (weight%)	O (atomic%)	Error%
GO	53.72	60.72	5.23	46.28	39.28	9.91
B-rGO	71.31	76.80	4.38	28.69	23.20	13.01
W-rGO	80.57	84.64	3.11	19.43	15.33	11.36
C-rGO	71.77	77.20	4.13	22.80	28.23	12.61

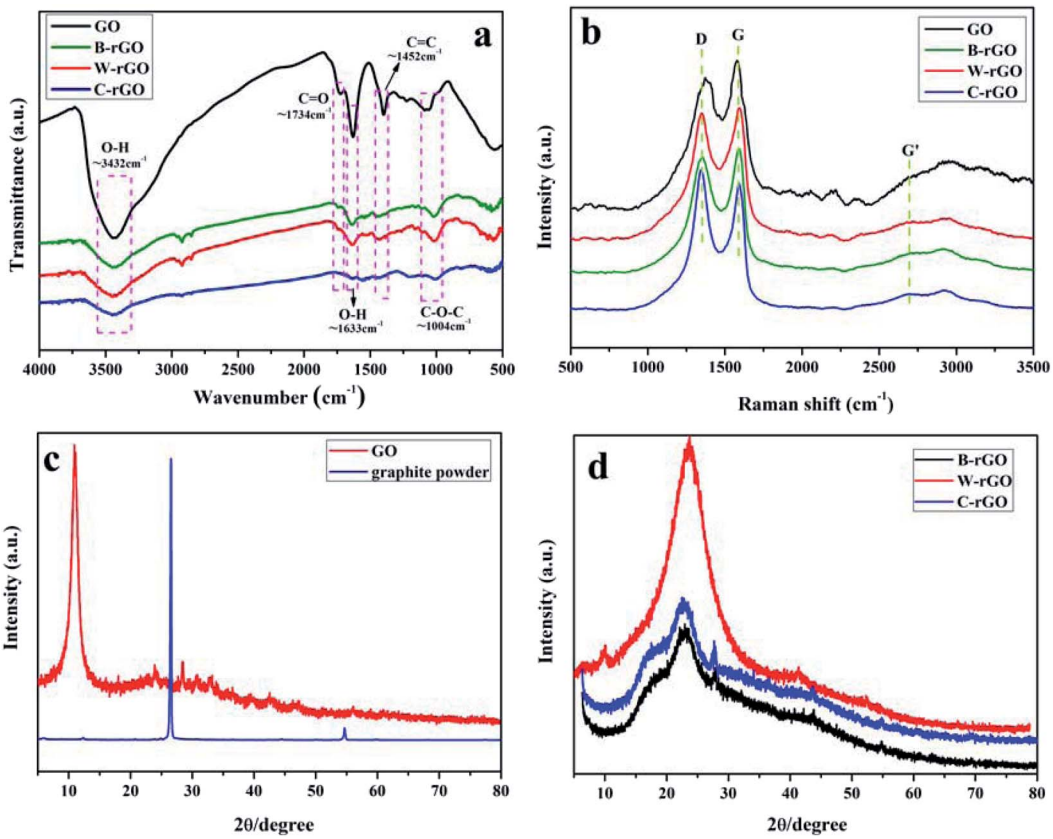

Fig. 4 (a) FT-IR spectrum and (b) Raman spectrum of GO, B-rGO, W-rGO and C-rGO, (c) XRD pattern of GO and graphite powder, (d) XRD pattern of B-rGO, W-rGO and C-rGO.

same time, the diffraction peak width of rGO increased due to the reduction of the size of rGO and the appearance of incomplete crystal structure. Compared to the XRD curves of three kinds of rGO, W-rGO has the highest peak intensity and the most complete reduction, while B-rGO and C-rGO has other small diffraction peaks, indicating that the number of layers is large.

3.1.3 XPS analysis of GO and rGO. The elemental composition and type of bond of rGO was characterized by XPS analysis. The full survey spectra and C 1s XPS spectrum of GO and rGO are illustrated in Fig. 5. Fig. 5(a), (c), (e) and (g) revealed that GO and rGO mainly contained C and O elements and the peaks of C 1s and O 1s appear at ~284.9 eV and ~531.4 eV, respectively. Fig. 5(b), (d), (f) and (h) showed four peaks of the C 1s XPS spectrum, which was fitted into sp^2 and sp^3 hybridized carbon atoms in C–C/C=C (~284.1 eV), C–O (~285.7 eV), a carboxyl group (–COOH) at ~287.2 eV and O=C–O (288.2 eV), separately. By comparing the full survey spectra of GO and rGO, it can be found that the content of O element of unreduced GO was relatively high, which was related to a large amount of C=O bonds. The content of O element in the three rGO was reduced, which was attributed to the reduction of reducing agent. However, it could be seen that the reduction was not complete due to the limited reduction components of the reducing agent, which was consistent with the test results of FT-IR spectrum.

3.1.4 Particle size distribution of three-ecofriendly rGO. In addition, the particle size distributions were analyzed using a particle size analyzer (Fig. 6). The particle sizes of the three kinds of rGO approximately distributed between 0.12 and 0.37 μm. Besides, Fig. 6(b) displays 59% of the particle of W-rGO nanofluids were concentrated in the range of 0.25–0.29 μm, with concentrated and uniform particle sizes. The more concentrated and uniform the particle size of W-rGO nanofluid is, the more stable the nanofluid is. This may be due to the similar forces in all directions, nanoparticles can be steadily suspended in the base fluid, and the macro performance of nanofluid is satisfactory stability.

3.1.5 Mechanism analysis of three-ecofriendly of rGO. Beer, wine and cocoa are three food-grade raw materials. Beer is brewed through liquid fermentation of wheat malt, barley malt and hops. According to reports, the natural sources of antioxidants in beer are biocompatible phenolic compounds, mainly composed of compounds such as eugenic acid, protocatechin, tannic acid, epicatechin and quercetin, which are excellent antioxidants because they react easily with reactive oxygen species (such as free radicals).[20] Wine is an alcoholic beverage made from fresh grapes or grape juice through complete or partial fermentation. The reducing substances are mainly tannins. According to reports, cocoa extract contains antioxidant flavonoids (quercetin is one of them), which can prevent the chemical process of cholesterol-induced arterial disease.[39,40]

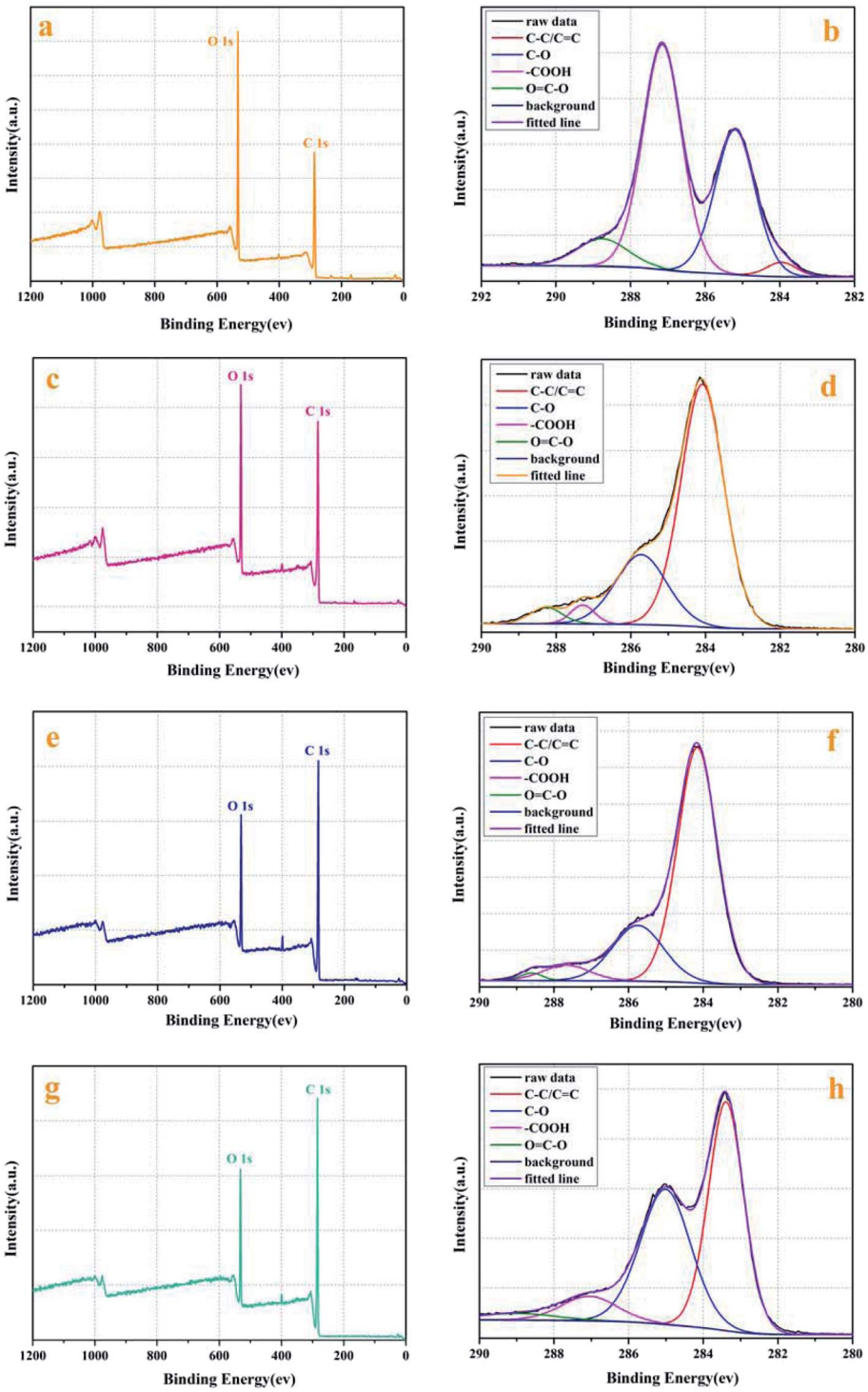

Fig. 5 XPS of (a) and (b): GO, (c) and (d): B-rGO, (e) and (f): W-rGO and (g) and (h): C-rGO.

Their mechanism of action as antioxidants generally is to remove free radicals through electron transfer and convert phenols to phenoxy.[41] While GO is covered with hydroxyl, epoxy, carbonyl and carboxyl groups, the hydroxyl and epoxy groups first absorb electrons in the environment to complete dehydration in the reduction process. The reaction mechanism of the three green reducing agents is shown in Fig. 7.

3.2 Performance analysis applied in nanofluids

3.2.1 Stability analysis of three kinds of rGO nanofluids. Since rGO has excellent thermal conductivity, it is widely used in the field of nanofluids. Therefore, the thermal conductivity and wettability of three kinds of nanofluids prepared by rGO were analyzed in this paper. The three kinds of rGO powders were separately dispersed in three kinds of water/ethanol

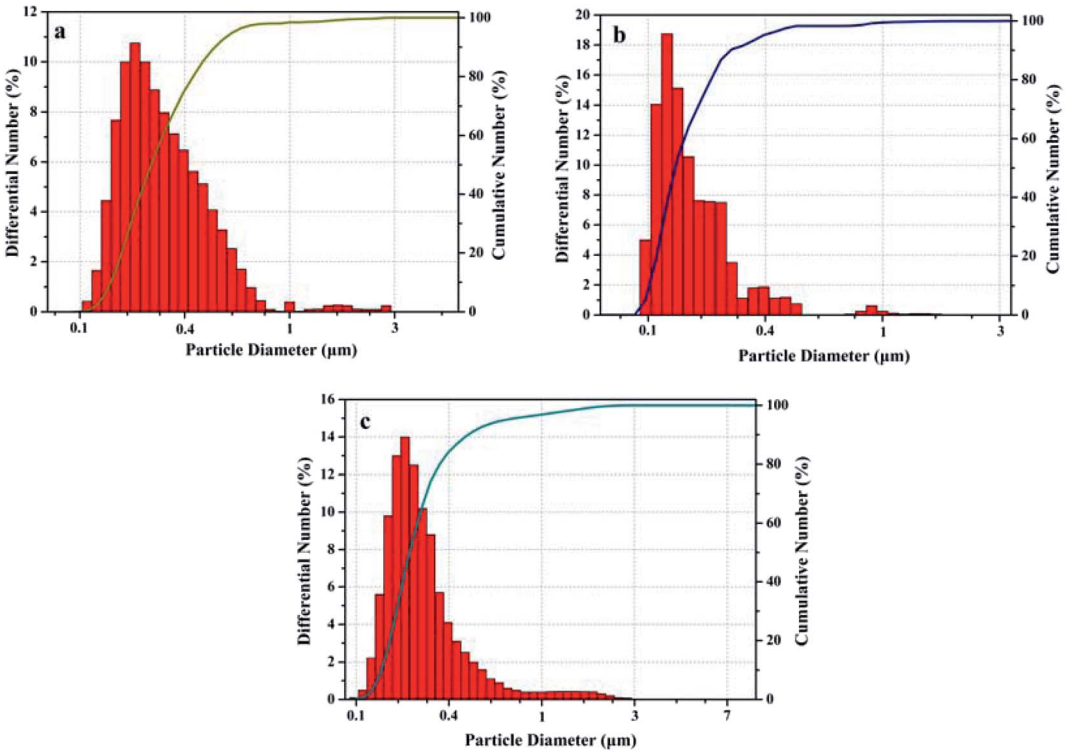

Fig. 6 Particle size distribution: (a) B-rGO, (b) W-rGO, (c) C-rGO.

mixed-based fluids (the volume ratios of water and ethanol were 25 : 75, 50 : 50 and 75 : 25, respectively) to obtain rGO nanofluids with a concentration of 0.1 mg ml^{-1}. Furthermore, in the process of preparing rGO nanofluids, rGO were mixed with the base fluids according to a certain concentration, and at room temperature for 15 min in the ultrasonic dispersion of ultrasonic vibration, to disperse the nanoparticles evenly and reduce agglomeration. In order to prevent adverse effects of excessive

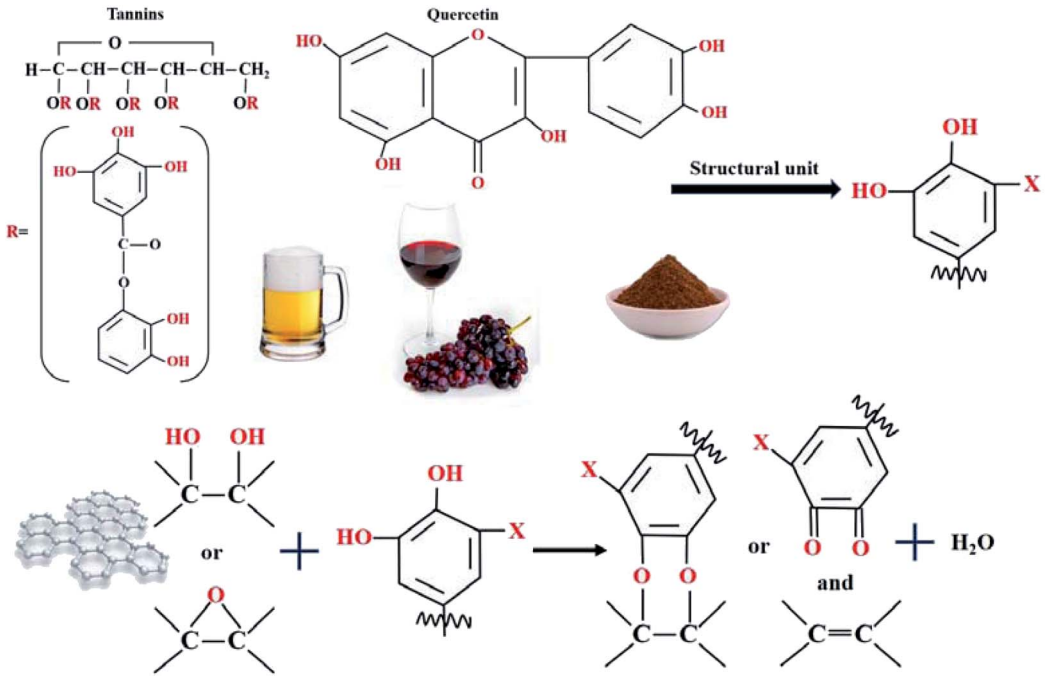

Fig. 7 Reaction mechanism diagram of preparation of rGO by main reducing agents in beer, wine and cocoa.

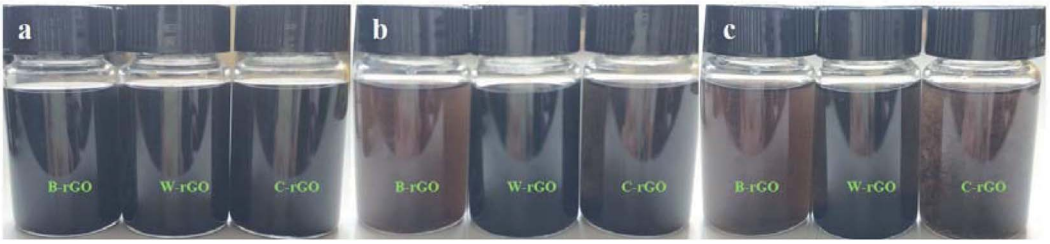

Fig. 8 Static diagram of three rGO nanofluids with a water/ethanol-based solution (25 : 75): (a) 10 days, (b) 20 days, (c) 30 days.

local temperature on nanofluids, the ultrasonic mode selected in the experiment was intermittent, with ultrasonic every 60 s and ultrasonic time of one time being 60 s.

Excellent suspension stability is the basis for the application of nanofluids. In this paper, the stability of three rGO nanofluids was evaluated by natural sedimentation method and absorbance method. Fig. 8 displays the sedimentation results of three rGO nanofluids (from left to right are B-rGO nanofluids, W-rGO nanofluids and C-rGO nanofluids) with a water/ethanol-based solution (25 : 75) after standing for 10, 20 and 30 days, respectively. By comparison, it can be found that W-rGO nanofluids have no obvious precipitation phenomenon within 30 days, indicating its excellent stability, which is consistent with the results of particle size distribution.

To further characterize the dispersion of the three rGO nanofluids, the absorbance of rGO nanofluids was measured using an ultraviolet-visible spectrophotometer. Due to rGO splits at 270 nm in the UV-vis spectrum is mainly related to the two conjugation effects of the π–π^* conjugate system,[42,43] and its maximum absorption wavelength is located at 270 nm on the UV-vis spectrum (shown in Fig. 9(a)), therefore 270 nm was selected for measurement. Fig. 9(b)–(d) display the absorbance of three rGO nanofluids in three water/ethanol mixed-based fluids varied with time. It can be found that within 30 days, the absorbance of rGO nanofluids decreased slightly, indicating that the prepared rGO nanofluids were relatively stable. In addition, in the three water/ethanol mixed-based fluids, W-rGO nanofluids had the smallest change in absorbance within 30 days, with rates of change of about 3.6%, 7.27% and 3.63%,

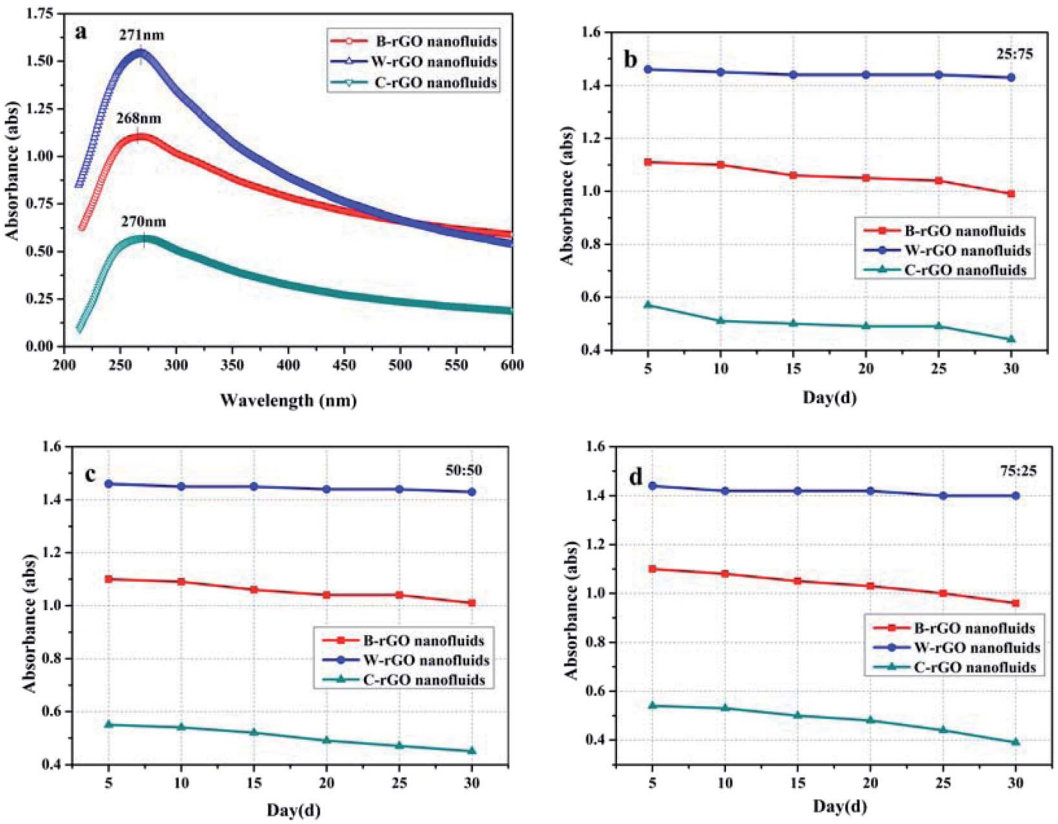

Fig. 9 (a) UV-visible spectrum of rGO nanofluids, the absorbance of rGO nanofluids in three water/ethanol ratio base solutions varied with time: (b) 25 : 75, (c) 50 : 50, (d) 75 : 25.

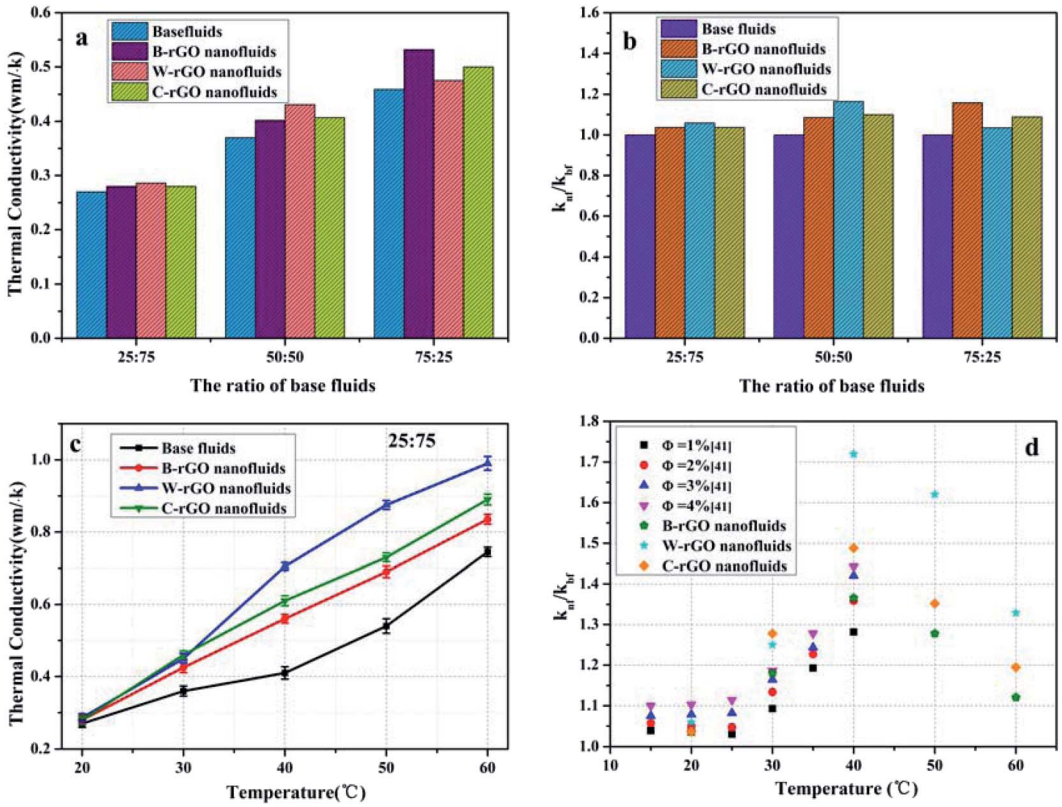

Fig. 10 (a) Thermal conductivity of four fluids at 25 : 75, 50 : 50 and 75 : 25 water/ethanol-based fluids ratios, (b) thermal conductivity ratio of the three rGO nanofluids to base fluids, (c) the tendency of thermal conductivity of four fluids at 25 : 75 water/ethanol-based fluids ratios with temperature, (d) comparison of experimental data and literature data at different temperature.

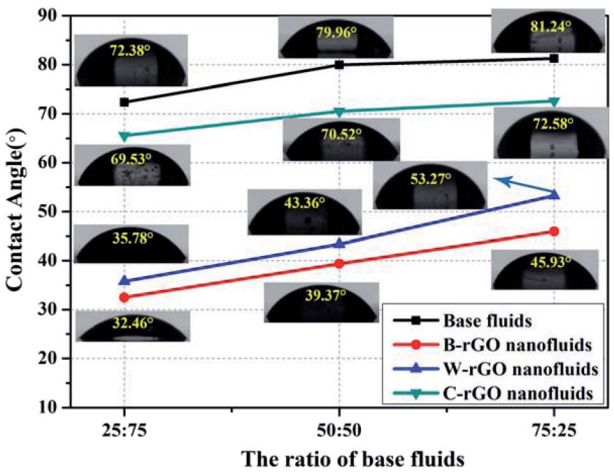

Fig. 11 Contact angle of base fluids and rGO nanofluids at different ratios of water–ethanol mixed-based fluids.

respectively, indicating that W-rGO nanofluids had the best stability, which is consistent with the results of the static figure in Fig. 8.

3.2.2 Thermal conductivity analysis of rGO nanofluids. Thermal conductivity is one of the primary indicators for exploring the thermal properties of nanofluids. Fig. 10(a) describes the thermal conductivity of base fluids and three rGO nanofluids with the ratios of 25 : 75, 50 : 50, and 75 : 25 water/ethanol mixed-based fluids at room temperature. The thermal conductivity of rGO nanofluids is higher than that of the base fluids. Fig. 10(b) displays the thermal conductivity ratio of the rGO nanofluids to base fluids. As we can see, the thermal conductivity ratio of W-rGO nanofluids is 1.165 at the ratio of 50 : 50, while the ratio of B-rGO nanofluids is 1.159 at the ratio of 75 : 25. Furthermore, the tendency of thermal conductivity of four fluids with temperature at 25 : 75 water/ethanol-based fluids ratios were analyzed (Fig. 10(c)). The Brownian motion of the rGO sheet layer inside the nanofluid becomes intense with the increase of temperature, and the microconvection between it and the base fluid is enhanced, which accelerates the energy transfer. Therefore, the thermal conductivity of the rGO nanofluids increases with the increase of temperature. Fig. 10(d) compares the experimental data with the references data.[41] It can be seen that both the experimental data and the reference data show the maximum value of k_{nf}/k_{bf} at 40 °C, indicating that the thermal conductivity increases the most and the heat transfer effect is the best at 40 °C, and the experimental data is also higher than the data in the reference, which indicates the rGO nanofluids in the experiment have better heat transfer effect.

3.2.3 Contact angle analysis of rGO nanofluids. The contact angle of the nanofluids is an indicator of the wettability of the nanofluid on the surface of the solid substrate, and is

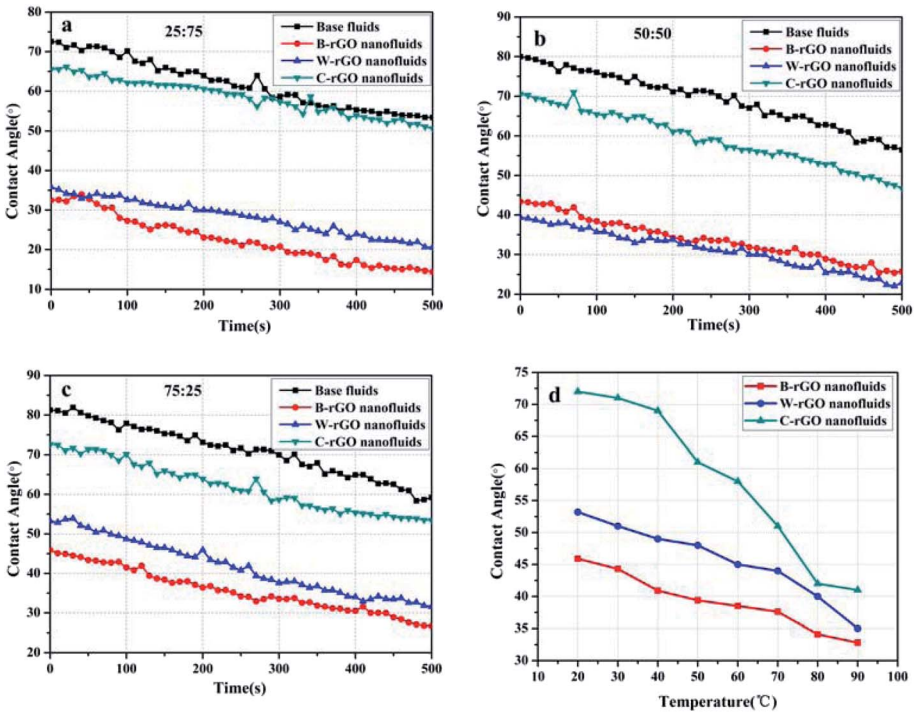

Fig. 12 The trend of contact angle with time: (a) 25 : 75, (b) 50 : 50, (c) 75 : 25, (d) the trend of contact angle with temperature.

related to the surface energy. At the same time, the contact angle of the nanofluids has a certain degree of influence on the heat transfer performance of the nanofluids. Chinnam *et al.*[44] experimentally revealed the influence of nanoparticles on droplets fixed on the substrate surface. For convenience, solid particles in the nanofluids are simplified into spheres, which are larger, denser and heavier than the base fluids molecules. The nanoparticle exerts an additional downward force on the droplet, squeezing the droplet towards the solid surface, so the contact angle will decrease when the nanoparticle is added to the base fluids. Fig. 11 describes the contact angle of base fluids and three rGO nanofluids. As can be seen from Fig. 11, the contact angle of the base fluids decreases to a certain extent with the addition of rGO. Among them, the contact angle of B-rGO nanofluids decreased the most, and the order of decrease degree was B-rGO nanofluids > W-rGO nanofluids > C-rGO nanofluids. For example, the contact angle of B-rGO nanofluids on the base fluids decreases by 55.59%, 49.54% and 44.35% at the ratio of water to ethanol-based fluids is 25 : 75, 50 : 50 and 75 : 25, respectively. It can be seen that the wettability of B-rGO nanofluids with water–ethanol mixed-based fluids ratio is preferably. While it intuitively observed from Fig. 11 that the contact angle of the nanofluids with different base fluids ratios changes, and the contact angle increases with the increase of the proportion of water in the base fluids.

At room temperature, the contact angle of different fluids with ratios of 25 : 75, 50 : 50 and 75 : 25 was measured over time. The trend is shown in Fig. 12(a)–(c). As you can see, with the increase of time, the contact angle of the four fluids decreases gradually, and the decrease degree of the contact angle of the effluent was larger than that of the nanofluids in the three different water–ethanol ratio fluids. For example, in the 25 : 75 ratio of water–ethanol mixed-based fluids, the decrease rate of base fluids is 0.038° s^{-1}, while the rate of B-rGO nanofluids, W-rGO nanofluids and C-rGO nanofluids is 0.036° s^{-1}, 0.0334° s^{-1} and 0.0297° s^{-1}, respectively, which is seem to related to the interaction between the nanoparticles and the base fluids in the nanofluids. It has been reported to analyze the relationship between dynamic contact angle and time.[45] Furthermore, temperature is an important factor, which can affect the contact angle of nanofluids. Taking three rGO nanofluids with a water–ethanol ratio of 75 : 25 as an example, the change in contact angle at different temperature was measured, and the effect of temperature on contact angles was explored. Fig. 12(d) shows the contact angle of B-rGO nanofluids, W-rGO nanofluids and C-rGO nanofluids at different temperature. As the temperature increases, the contact angle of the three rGO nanofluids all decreases. In general, the higher the temperature, the more violent the movement of nanoparticles in the nanofluids, the stronger the fluidity of the nanofluids, and the smaller the contact angle. The reduction degree in the contact angle of B-rGO nanofluids is the smallest, and the affection of temperature is the least, which indicating that B-rGO nanofluids can better adapt to the temperature change in the heat transfer process.[44]

4. Conclusion

Beer, wine and cocoa were used as green reductants to prepare three kinds of rGO successfully through REDOX method, and the differences in microstructure and stability of these rGO were

analyzed due to the different reductants. The analysis results show that the three kinds of rGO have certain differences in particle size distribution and stability, in which W-rGO particle size distribution is more concentrated, and the stability is relatively excellent within 30 days. Furthermore, nine rGO nanofluids were prepared using mixtures of different volume ratios of water and ethanol (25 : 75, 50 : 50 and 75 : 25) as the base fluids, and the thermal conductivity and wetting properties of the rGO nanofluids were characterized. When water–ethanol volume ratio is 25 : 75 and 50 : 50, W-rGO nanofluids have a relatively good thermal conductivity, while B-rGO nanofluids have the best thermal conductivity when the volume ratio is 75 : 25. Therefore, the thermal conductivity of the nanofluids is affected not only nanoparticles but also base fluids. In addition, the contact angle of rGO nanofluids decreases with the increase of time and temperature. It seems that the decrease degree of contact angle is different due to the different force of different nanoparticles on the base fluids.

Conflicts of interest

There are no conflicts to declare.

Acknowledgements

This research is support by the National Natural Science Foundation of China-Shandong Joint Fund (No. U1806222) and the Natural Science Foundation of Shandong Province (No. ZR2016QL004).

References

1 K. S. Novoselov, A. K. Geim, S. V. Morozov, D. Jiang, Y. Zhang, S. V. Dubonos, I. V. Grigorieva and A. A. Firsov, *Science*, 2004, **306**(66), 6–9.
2 C. Zhu, D. Du and Y. Lin, *Biosens. Bioelectron.*, 2017, **89**, 43–55.
3 C. A. Ubani, M. A. Ibrahim, M. A. M. Teridi, K. Sopian, J. Ali and K. T. Chaudhary, *Sol. Energy*, 2016, **137**, 531–550.
4 A. Nélia, V. César, D. Daniel, A. F. A. Nuno, G. Gil, L. P. João, A. A. P. M. Paula, N. Rogério and N. Victor, *Mater. Today: Proc.*, 2015, **2**, 171–177.
5 O. Yasin, K. Hossein, A. Omid, A. Mahnaz, H. Shilan, K. Salah and S. N. Masoud, *J. Alloys Compd.*, 2020, **848**, 156495.
6 Š. Václav, H. Jiří, B. Jana, E. Petra and K. Martin, *Ultrason. Sonochem.*, 2015, **24**, 65–71.
7 X. Li, L. Colombo and R. S. Ruoff, *Adv. Mater.*, 2016, **28**, 6247–6252.
8 Y. Shi, C. Hamsen, X. Jia, K. K. Kim, A. Reina, M. Hofmann, A. L. Hsu, K. Zhang, H. Li, Z. Y. Juang, M. S. Dresselhaus, L. J. Li and J. Kong, *Nano Lett.*, 2010, **10**, 4134–4139.
9 C. Lin, L. Yang, L. Ouyang, J. Liu, H. Wang and M. Zhu, *J. Alloys Compd.*, 2017, **728**, 578–584.
10 C. A. Amarnath, C. E. Hong, N. H. Kim, B. C. Ku, T. Kuila and J. H. Lee, *Carbon*, 2011, **49**, 3497–3502.
11 S. Wakeland, R. Martinez, J. K. Grey and C. C. Luhrs, *Carbon*, 2010, **48**, 3464–3470.
12 Z. Fan, K. Wang, T. Wei, J. Yan, L. Song and B. Shao, *Carbon*, 2010, **48**, 1686–1689.
13 W. S. Hummers and R. E. Offeman, *J. Am. Chem. Soc.*, 1958, **80**, 1339.
14 S. Stankovich, D. A. Dikin, R. D. Piner, K. A. Kohlhaas, A. Kleinhammes, Y. Jia, Y. Wu, S. T. Nguyen and R. S. Ruoff, *Carbon*, 2007, **45**(7), 1558–1565.
15 H. J. Shin, K. K. Kim, A. Benayad, S. M. Yoon, H. K. Park, I. S. Jung, M. H. Jin, H. K. Jeong, J. M. Kim, J. Y. Choi and Y. H. Lee, *Adv. Funct. Mater.*, 2009, **19**(12), 1987–1992.
16 D. Chen, L. Li and L. Guo, *Nanotechnology*, 2011, **22**, 325601.
17 Y. Jin, S. Huang, M. Zhang, M. Jia and D. Hu, *Appl. Surf. Sci.*, 2013, **268**, 541–546.
18 K. Tewatia, A. Sharma, M. Sharma and A. Kumar, *Mater. Today: Proc.*, 2021, **44**, 3933–3938.
19 S. W. Chong, C. W. Lia and S. B. A. Hamid, *Ceram. Int.*, 2015, **41**, 9505–9513.
20 A. T. Mahmoud, T. Azam, D. Vivek, Y. R. Kyong and S. J. Park, *J. Ind. Eng. Chem.*, 2014, **20**, 4327–4331.
21 Z. J. Fan, W. Kai, J. Yan, T. Wei, L. J. Zhi, J. Feng, Y. Ren, L. P. Song and F. Wei, *ACS Nano*, 2011, **5**(1), 191–198.
22 Z. Bo, X. Shuai, S. Mao, H. Yang, J. Qian, J. Chen, J. Yan and K. Cen, *Sci. Rep.*, 2014, **4**, 4684.
23 H. Cheng, J. Lin, Y. Su, D. Chen, X. Zheng and H. Zhu, *Mater. Today Commun.*, 2020, **23**, 100938.
24 J. Liu, S. Fu, B. Yuan, Y. Li and Z. Deng, *J. Am. Chem. Soc.*, 2010, **132**(21), 7279–7281.
25 M. Mahmudzadeh, H. Yari, B. Ramezanzadeh and M. Mahdavian, *J. Ind. Eng. Chem.*, 2019, **78**, 125–136.
26 X. Li, Y. Chen, Z. Cheng, L. Jia, S. Mo and Z. Liu, *Appl. Energy*, 2014, **130**(5), 824–829.
27 R. Sadri, M. Hosseini, S. Kazi, S. Bagheri, N. Zubir, G. Ahmadi, M. Dahari and T. Zaharinie, *Chem. Phys. Lett.*, 2017, **675**, 92–97.
28 M. Mehrali, E. Sadeghinezhad, M. M. Rashidi, A. R. Akhiani, S. T. Latibari, M. Mehrali and H. S. C. Metselaar, *J. Nanopart. Res.*, 2015, **17**(6), 267.
29 M. Mohammad, S. Emad, A. Reza, R. A. Amir, T. L. Sara, M. Mehdi and S. C. M. Hendrik, *Energy Convers. Manage.*, 2016, **118**, 459–473.
30 Y. P. Hu, Y. R. Li, L. Lu, Y. J. Mao and M. H. Li, *Int. J. Therm. Sci.*, 2020, **152**, 106309.
31 V. V. Wanatasanapan, M. Z. Abdullah and P. Gunnasegaran, *J. Mater. Res. Technol.*, 2020, **9**, 13781–13792.
32 T. J. Choi, S. H. Kim, S. P. Jang, J. D. Yang and Y. M. Byeon, *Appl. Therm. Eng.*, 2020, **180**, 115780.
33 S. N. Abbas Shah, S. Shahabuddin, M. F. Mohd Sabri, M. F. Mohd Salleh, A. M. Ali, N. Hayat, N. A. Che Sidik, M. Samykano and R. Saidur, *Int. J. Heat Mass Transfer*, 2020, **150**, 118981.
34 K. Kanishka, H. D. Silva, H. H. Huang and M. Yoshimura, *Appl. Surf. Sci.*, 2018, **447**, 338–346.
35 T. Kuila, S. Bose, P. Khanra, A. K. Mishra, N. H. Kim and J. H. Lee, *Carbon*, 2012, **50**, 914–921.
36 Z. Ma, P. Song, Z. Yang and Q. Wang, *Appl. Surf. Sci.*, 2019, **465**, 625–634.

37 K. Wang, Q. Ma, K. Pang, B. Ding, J. Zhang and Y. Duan, *Carbohydr. Polym.*, 2018, **194**, 146–153.
38 H. R. Zhao, B. Y. Xu, J. H. Ding, Z. Wang and H. B. Yu, *ACS Sustainable Chem. Eng.*, 2019, **7**(23), 18819–18825.
39 R. Kamatchi and G. Kumaresan, *Chin. J. Chem. Eng.*, 2018, **26**, 445–454.
40 B. E. Mary and M. E. Marguerite, *Nutr. Res.*, 2004, **24**, 695–706.
41 M. Mohammad, S. Emad, R. A. Amir, T. L. Sara, T. Sepehr, D. P. Alireza, C. M. Hendrik Simon and M. Mehdi, *J. Cleaner Prod.*, 2016, **137**, 555–566.
42 S. Coe, E. Axelsson, V. Murphy, M. Santos, J. Collett, M. Clegg, H. Izadi, J. M. Harrison, E. Buckingham and H. Dawes, *Clin. Nutr. ESPEN*, 2017, **21**, 20–25.
43 Y. L. Xu, H. X. Li, C. B. Zhou, X. S. Xiao, Z. C. Bai, Z. P. Zhang and S. J. Qin, *Optik*, 2020, **219**, 165015.
44 J. Chinnam, D. Das, R. Vajjha, R. Vajjha and J. Satti, *Int. Commun. Heat Mass Transfer*, 2015, **62**, 1–12.
45 M. J. Vega, D. Seveno, G. Lemaur, M. H. Adao and J. De Coninck, *Langmuir*, 2005, **21**, 9584–9590.